

## Feasibility of forest-fire smoke detection using lidar

*Andrei B. Utkin<sup>A,B</sup>, Armando Fernandes<sup>C</sup>, Fernando Simões<sup>C</sup>, Alexander Lavrov<sup>A</sup>  
and Rui Vilar<sup>C,D</sup>*

<sup>A</sup>INOV-Inesc Inovação, Rua Alves Redol 9, 1000-029 Lisbon, Portugal.

<sup>B</sup>Telephone: +351 213 100 426; fax: +351 213 100 401; email: andrei.utkin@inov.pt

<sup>C</sup>Departamento de Engenharia de Materiais, Instituto Superior Técnico, Av. Rovisco Pais 1, 1049-001, Lisbon, Portugal.

<sup>D</sup>Telephone: +351 218 418 120; fax: +351 218 418 121; email: rui.vilar@ist.utl.pt

**Abstract.** The feasibility and fundamentals of forest fire detection by smoke sensing with single-wavelength lidar are discussed with reference to results of 532-nm lidar measurements of smoke plumes from experimental forest fires in Portugal within the scope of the Gestosa 2001 project. The investigations included tracing smoke-plume evolution, estimating forest-fire alarm promptness, and smoke-plume location by azimuth rastering of the lidar optical axis. The possibility of locating a smoke plume whose source is out of line of sight and detection under extremely unfavourable visibility conditions was also demonstrated. The eye hazard problem is addressed and three possibilities of providing eye-safety conditions without loss of lidar sensitivity (namely, using a low energy-per-pulse and high repetition-rate laser, an expanded laser beam, or eye-safe radiation) are discussed.

**Additional keywords:** remote sensing, Gestosa.

### Introduction

Extending the principles of radar to the optical range, lidar (LIght Detection And Ranging) technology has found use in many of today's forestry applications, such as monitoring and measuring the chemical activities and status of trees and forests (Saito *et al.* 2000), and leaf-area estimation (Roberts *et al.* 2003). Lidar is also a promising tool for forest-fire monitoring because, due to its very high sensitivity and spatial resolution, this active detection technique enables efficient location of small smoke plumes that originate from forest fires in the early stages of development during both day and night over a considerable range (tens of kilometres). By using suitable rastering methods, very accurate location of the smoke source is also possible. The observation of smoke produced by power plants, factories, and forest fires was amongst the first applications of lidar (Hamilton 1969; Hinkley 1976). Since those early experiments, interest in lidar has steadily increased and lidar methods, along with sophisticated algorithms for lidar signal processing (Zuev and Naats 1983; Bissonnette 1986; Weinman 1988; Wei *et al.* 2001), are now widely used for atmospheric research and monitoring (Measures 1984; Jelalian 1992; Bösenberg *et al.* 1997). Most of these algorithms are based on an inversion method published by Klett (1981).

The use of lidar as a fire detection tool has yet to receive due attention. The few investigations reported recently are mostly concerned with large phenomena on both spatial and

temporal scales, such as on-ground and airborne evaluation of smoke clouds resulting from large forest fires (Uthe *et al.* 1982; Banta *et al.* 1992; Targ *et al.* 1996; Pershin *et al.* 1999), weapon firing exercises (Uthe 1981), tracking of oil smoke plumes (Eberhard 1983), measuring forest-fire smoke density in the atmosphere and stratosphere (Fromm *et al.* 2000; Muller *et al.* 2000), and investigating the correlation between smoke and ozone concentration (Longo *et al.* 1999). Local observations are predominantly focused on plumes emitted by power plants (Benech *et al.* 1988; Bennet *et al.* 1992). Thus, although smoke detection by lidar is a well-known technique, considerable effort is still required to create effective, reliable, and simple methods for ground-based forest fire surveillance. Numerical assessment of the lidar parameters required for successful use of lidar for fire detection was carried out by Andreucci and Arbolino (1993a, 1993b) and Vilar and Lavrov (1999, 2000). Earlier experiments carried out by the authors testify that small fires with a burning rate of about 0.03 kg of wood per second can be promptly detected from a distance of 6.5 km (Utkin *et al.* 2002).

The present paper partially addresses problems arising from the high cost and complexity of common lidar equipment by experimentally investigating the possibility of using a simple single-wavelength direct-detection lidar to locate forest fires. This possibility is closely related to the detection sensitivity of the device. Being an active technique, lidar-assisted detection of forest fires has the potential to reveal

forest fires in their earliest stages, when the burning area is small enough for the fire to be easily extinguished. Instead of observing the flames, lidar detects the smoke plume, which is much larger and higher. In the next section the fundamentals of smoke sensing using lidar are briefly discussed and the signal-to-noise ratio (*SNR*) is related to the parameters of the lidar equipment, smoke plume, and atmospheric conditions. This relation allows theoretical predictions of the SNR for ideal observation conditions to be made, when the probing laser beam irradiates the centre of a plume with constant shape. The results of experiments, designed to demonstrate the possibility of forest fire detection by lidar in a mountain region, even when the smoke plume is observed under strong wind against a steep hillside, are reported in the section entitled *Experimental results*. It is shown that even an inexpensive medium-spatial-resolution lidar can reliably differentiate the signal resulting from a small smoke plume from large signals due to ground reflections.

Another important characteristic of a lidar surveillance system is the promptness of the fire alarm. The experiments have demonstrated the possibility of detecting smoke plumes as early as 40 s after the fire starting. Forest fire location was performed by an azimuth-angle sweep, allowing the position and dimensions of the smoke plume to be estimated. Examples of location of a smoke plume whose origin is out of line of sight and detection under unfavourable visibility conditions were also demonstrated. The results are summarised in the final section.

## Fundamentals of smoke sensing

### Lidar signal

The power  $P_r$  received by the lidar is defined by the lidar equation (Measures 1984, p. 243):

$$P_r(R) = E_p \frac{c\langle\beta(R)\rangle}{2} \frac{A_r}{R^2} \tau_t \tau_r \exp\left(-2 \int_0^R \alpha(R') dR'\right), \quad (1)$$

where  $R$  is the current distance,  $E_p$  the output laser pulse energy,  $c$  the speed of light,  $\langle\beta(R)\rangle$  the mean backscattering coefficient,  $A_r$  the effective receiver area,  $\tau_t$  and  $\tau_r$  the transmitter and receiver efficiencies (the latter essentially defined by a filter confining the receiver bandwidth), and  $\alpha$  the extinction coefficient. The calculation of the backscattering coefficient  $\langle\beta\rangle$  takes into consideration smoke dilution due to mixing with air. It is averaged over the area illuminated by the laser beam as well as along the line of sight within the range  $ct_p/2$ , where  $t_p$  is the laser pulse duration (for a pulse of 10 ns the distance of averaging is 1.5 m). The extinction coefficient  $\alpha$  was estimated by the slope method (Klett 1981; Zuev and Naats 1983) from the lidar signals recorded in a smoke-free atmosphere, immediately before and after each series of experiments.

The smoke plumes from forest fires in the initial stage are compact rather than dispersed targets. They appear in the raw

lidar signal as narrow peaks and in this condition the most useful measure of detection efficiency is the ratio between the peak return signal value and the background noise in the vicinity of the peak.

### Noise

Fluctuations in the return lidar signal arise due to atmospheric effects and noise associated with the optical detection system. The output signal from the photomultiplier includes three components (Measures 1984, pp. 226–233; Andreucci and Arbolino 1993b): the current due to the received laser beam energy,  $I_{sig} = P'_r R_p G$ , the current resulting from background radiation,  $I_{bgnd} = P_{bgnd} R_p G$ , and the dark current  $I_{dark}$ . In the above equations,  $P'_r$  is the power of received backscattered radiation in the vicinity of the signal peak,  $G$  the photomultiplier gain,  $R_p$  the photocathode responsivity and  $P_{bgnd}$  the power of received background solar radiation (Youmans *et al.* 1994). The latter is given by:

$$P_{bgnd} = A_r \tau_r B_f \frac{\pi \gamma^2}{4} L_\lambda, \quad (2)$$

where  $B_f$  is the receiver optical bandwidth confined by an optical filter,  $\gamma$  is the full angle of field of view, and  $L_\lambda$  is the background solar radiance at the lidar operating wavelength.

When data are accumulated over  $n$  lidar shots, the signal-to-noise ratio is defined by the equation (Measures 1984, pp. 226–229):

$$\begin{aligned} SNR &= \frac{P_r R_p G \sqrt{n}}{\sqrt{2eG^2 F B_e (P'_r R_p + P_{bgnd} R_p + I_{dark}/G)}} \\ &= P_r R_p \sqrt{\frac{n}{2e F B_e (P'_r R_p + P_{bgnd} R_p + I_{dark}/G)}}, \end{aligned} \quad (3)$$

where  $e$  is the electron charge,  $B_e$  the effective bandwidth of the receiver, and  $F$  the noise factor associated with the gain.

## Experimental results

Experimental investigations on the detection of small forest-fire smoke plumes were carried out using a direct-detection lidar operating with visible radiation of 532 nm wavelength. The backscattered radiation was collected by a Cassegrainian-type telescope and measured by a photomultiplier. The experimental lidar curves correspond to the accumulation of  $n = 128$  return signals. Relevant parameters of the lidar equipment used for the experiments are presented in Table 1. The value of the background solar radiance given in Table 1 was obtained by interpolation of data available in the literature (Pratt 1969; Youmans *et al.* 1994).

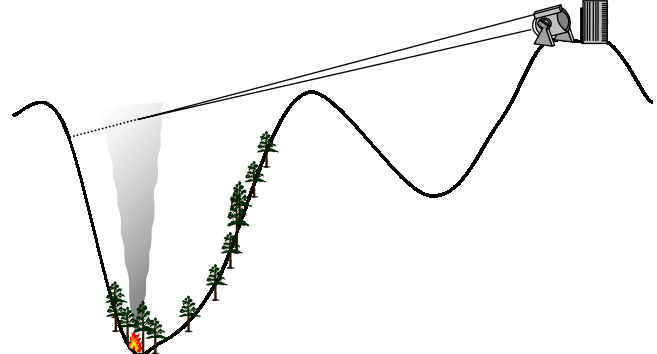
These experiments, which aimed to demonstrate the basic principles and feasibility of lidar-assisted smoke sensing, were performed using robust lidar equipment, capable of providing easy operation in the field. This apparatus is based

**Table 1.** Characteristics of the lidar set-up and the background solar radiance

Parameter	Notation	Units	Value
<b>Transmitter</b>			
<i>Flashlamp-pumped, water-cooled, Q-switched Nd:YAG laser</i>			
Pulse duration	$t_p$	ns	10
Repetition rate		Hz	1–15
Beam divergence		mrad	~0.5
Operating wavelengths	$\lambda$	nm	532
Estimation of pulse energy for the flashlamp voltage	$E_p$	mJ	Up to 20
Total transmitter efficiency	$\tau_t$	%	90
<b>Receiver</b>			
<i>Cassegrainian telescope</i>			
Effective area	$A_r$	$\text{m}^2$	0.0678
Full angle of field of view	$\gamma$	mrad	1.45
Efficiency	$\tau_r$	%	64
Filter bandwidth	$B_f$	nm	4.8
<i>Photomultiplier with Peltier cooling</i>			
Dark current	$I_{dark}$	A	$4 \times 10^{-7}$
Gain	$G$		$\sim 10^5$
Estimation of photocathode responsivity	$R_p$	$\text{mA W}^{-1}$	0.7
<b>Data acquisition system</b>			
<i>IBM-compatible PC with ADC ISA board</i>			
Frequency		Sample/s	$25 \times 10^6$
Corresponding space resolution		m	6
<b>Parameters of the atmosphere</b>			
Background solar radiance	$L_\lambda$	$\text{W m}^{-2} \text{sr}^{-1} \mu\text{m}^{-1}$	120

on a solid-state Nd:YAG laser, with a frequency-doubling non-linear crystal in order to provide easy-to-track green radiation, as well as the fundamental infrared radiation. The experiments were carried out in a protected area, so eye-safety conditions were unimportant in this context. The ways of providing eye-safety without significantly decreasing the detection range are discussed in the Conclusions.

Forest fire surveillance using lidar requires the equipment to be placed at elevated observation points in order to avoid masking of the area under surveillance by ground relief and foreground objects (trees, buildings, etc.). In Portugal, forests are predominantly located in mountain areas, where one can take advantage of the natural relief and place the observation stations on the top of mountains or on already existing surveillance towers. Since forest fires often occur in valleys or on hillsides, fire detection in mountain regions is characterised by the fact that usually only the upper, less dense, part of the smoke plume appears in the direct field of view of the instrument and, in many cases, the plume must be detected against a background resulting from the hillside rather than against a clear sky (Fig. 1). In view of these remarks, the present work aims to demonstrate that the sensitivity and spatial resolution of a simple lidar instrument is sufficient for early detection of forest-fire smoke plumes in the above conditions. Experiments on detection of plumes of experimental forest fires were carried out in 2001 in Central Portugal within the framework of the Gestosa project (Viegas 2000).

**Fig. 1.** Observation of a forest fire in a mountain region.

An example of a 10-min smoke plume evolution captured in the lidar signal is given in Fig. 2. The smoke plume, significantly inclined due to wind, was observed at a height of 25 m above the ground; the distance from the lidar apparatus to the fire location was about 2.4 km. According to the predictions of theoretical treatments of smoke propagation in the atmosphere (Davidson and Slawson 1982; Heikes *et al.* 1990; Netterville 1990), the fire was located about 100 m to one side of the smoke detection point. The peak corresponding to the smoke plume, observed at  $t = 180$  s after the start of the fire, is easily differentiated from the stronger but spatially separated signal due to the hillside located 30 to 70 m behind the plume. At  $t = 450$  s the absorption of laser radiation by the smoke

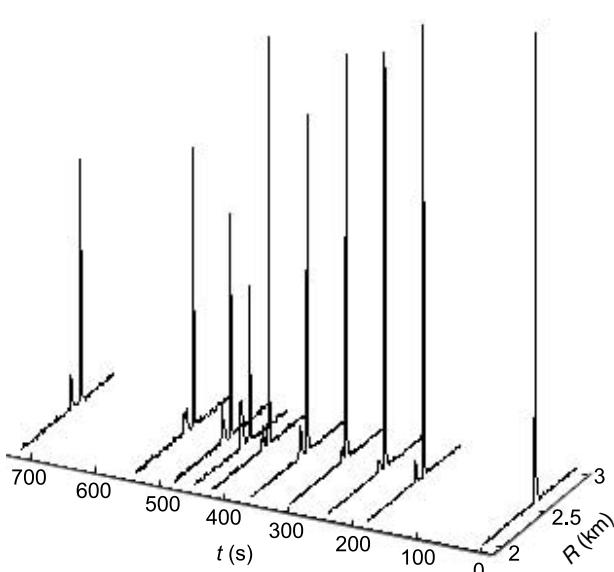


**Fig. 2.** Raw lidar signals reflecting evolution of the smoke plume against the hillside. Initial moment of time,  $t = 0$ , corresponds to the start of the fire,  $E_p = 2 \text{ mJ}$  and  $\nu = 15 \text{ Hz}$ .

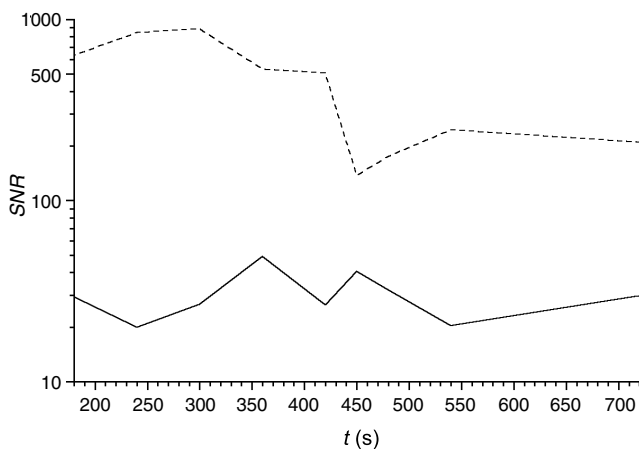


**Fig. 3.** Evolution of the smoke plume in terms of signal-to-noise ratio.  $SNR$  for the smoke-plume peak is shown as a solid line, for the hillside as a dashed one.

is so high that the signal from the hillside becomes 3 times weaker than at  $t = 0$ . A quantitative representation of the time dependence of the  $SNR$  for the plume and the hillside is given in Fig. 3. In lidar fire surveillance, typical observation conditions imply that segments of clear air constitute the greatest part of the probing pulse path in the atmosphere, so the signal peaks are surrounded by areas in which the backscattered radiation is small. Within these areas the signal curve may be approximated, with an error several times less than the noise level, by a straight line. Then the noise may be characterised by the standard deviation of the signal points with respect to this straight line.

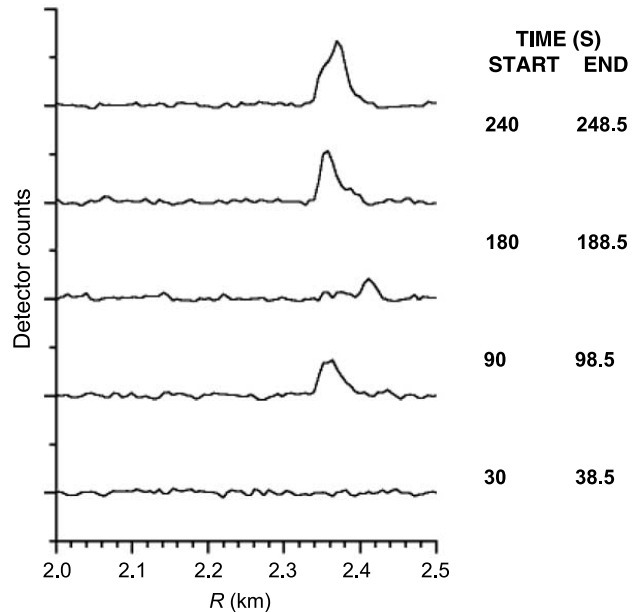


**Fig. 4.** Example of early detection of the smoke plume,  $E_p = 15 \text{ mJ}$ ,  $\nu = 15 \text{ Hz}$ .

Following this technique, the noise level in the experimental curves was estimated by analysing the behaviour of lidar return curves in 400 m regions (for the conditions in question, it is short enough for the signal curve to be quasi-linear while long enough for providing a representative noise sample) immediately before and after the signal peak. The time-averaged value  $SNR = 54$ , estimated theoretically using equations (1) and (3), is in good agreement with the experimental values. Developing in conditions of non-uniform wind, the smoke plume was subjected to significant random deviations while the direction of the probing laser beam remained fixed, which resulted in the signal instability and, eventually, in the scatter of  $SNR$  values observed in Fig. 3.

An important feature of any fire-surveillance system is how fast it can detect a fire. Figure 4 shows the evolution of the lidar signal for an experimental forest fire that started at  $t = 0$ . The fire was detected 40 s after the start. This detection delay corresponded to the time required for the initial dense smoke cloud to rise upward and laterally (due to wind) to the location where it met the probing laser beam, 80 m above and 150 m to the side (in the horizontal direction) of the fire location. Each of the curves plotted in Fig. 4 corresponds to a repetition rate  $\nu = 15 \text{ Hz}$ , so the total time required for detection is  $n/\nu = 8.53 \text{ s}$ .

In the experiments described in previous sections, the probing beam and the collecting optics were manually pointed at the smoke plume and kept stationary during signal acquisition. However, real fire-monitoring systems should reveal smoke plumes by automatic scanning within a defined solid angle, corresponding to a prescribed surveillance area.

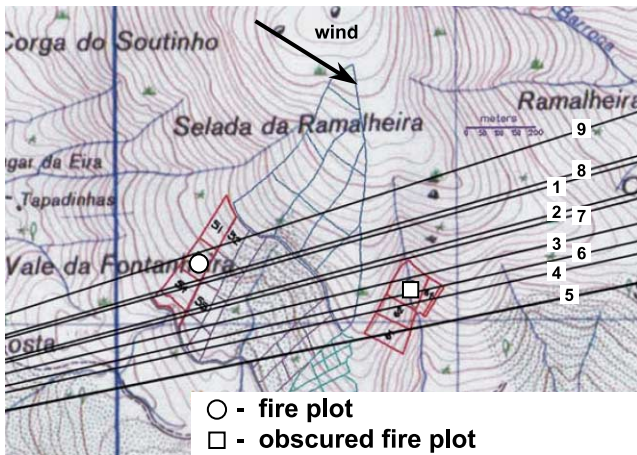


Fig. 5. Position of the scanning directions at fire plot site.

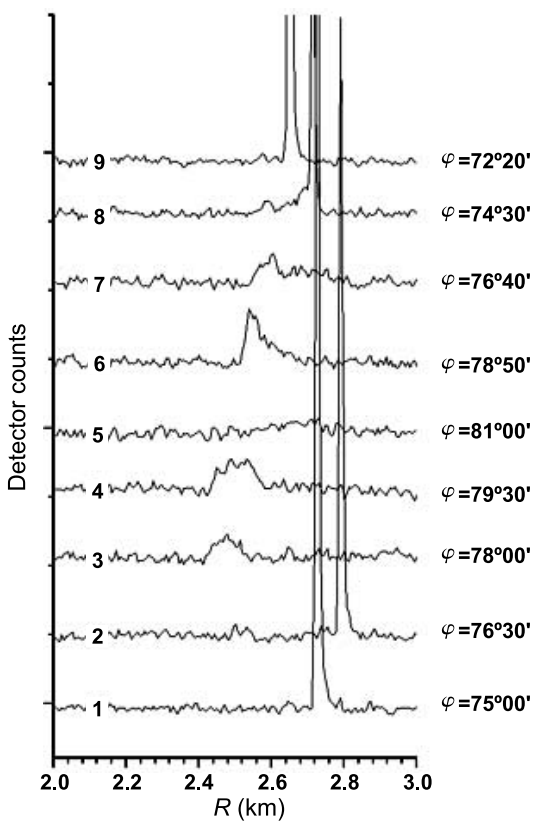


Fig. 6. Example of horizontal scanning,  $E_p = 15 \text{ mJ}$ ,  $\nu = 12 \text{ Hz}$ .

To demonstrate this ability, a two-pass equidistant azimuth sweep, from  $\varphi = 75^\circ$  to  $81^\circ$  with a step of  $1^\circ 30'$  and backward from  $\varphi = 81^\circ$  to  $72^\circ 20'$  with a larger step of  $2^\circ 10'$ , was performed. The azimuth angle  $\varphi$  is measured clockwise from the north direction, and the positions of the scanning beam with respect to the fire plot locality are shown in Fig. 5. The laser beam was in a horizontal plane about 80 m above the fire location.

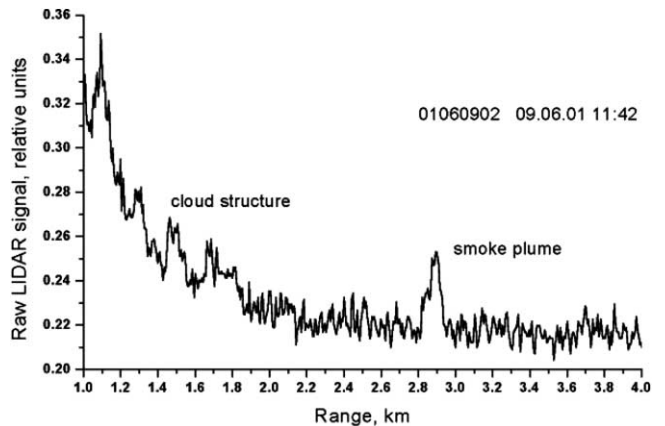


Fig. 7. Observation of the smoke plume through the cloud structure,  $E_p = 19 \text{ mJ}$ ,  $\nu = 15 \text{ Hz}$ .

The results of the scanning experiments are summarised in Fig. 6. At the beginning of the scanning ( $\varphi = 75^\circ$ ), the laser beam does not cross the plume, and only the strong signal backscattered from the hillside is seen (curve 1). With a one-step increase of  $\varphi$ , to  $76^\circ 30'$ , the probing laser beam enters the thinnest, external part of the plume, which appears in the signal (curve 2) by a peak with a near-threshold value of  $SNR \approx 2$ . Reliable smoke detection is achieved in the next scanning step of  $\varphi = 78^\circ$  (curve 3). For  $\varphi = 79^\circ 30'$  the laser beam goes above the lower hillside, so only the signal due to the smoke plume is observed in curve 4. A further increase of  $\varphi$  moves the laser beam outside the plume (curve 5). Backward scanning with a larger step leads to similar results. The maximum value of  $SNR = 17$  is achieved for  $\varphi = 76^\circ 40'$  (curve 7). A rough theoretical estimation of the SNR for the case in which the laser beam crosses the plume axis is 50. These results clearly demonstrate the possibility of fire detection by angular scanning. The method also allows the plume dimensions to be evaluated: about 120 m along the laser beam path and about 3 angular degrees cross-wise, which for a detection distance of 2.5 km corresponds to 130 m. The lidar signals were recorded with a repetition rate  $\nu = 12 \text{ Hz}$ , so for an automatic system with a  $2^\circ$  step the limiting time of full-circle scanning is as large as  $180 n / \nu = 32 \text{ min}$ . It should be noted that an easily achieved 10-fold increase of  $E_l$  or  $\nu$  leads to a duration of  $\sim 3 \text{ min}$  for a full-circle sweep.

One more characteristic of the lidar equipment, which is important for forest fire surveillance, especially in mountain regions, is its ability to function in a wide range of atmospheric conditions. Figure 7 illustrates a signal recorded in especially unfavourable weather conditions. Due to rain and dense fog the average visibility did not exceed 100 m. A better visibility of about 1 km was observed only within a 10-min interval during which the smoke plume from one of the obscured fire sites on the opposite hillside (marked by a square in Fig. 5) was detected. The signal of Fig. 7 clearly indicates the presence of a 100 m-thick smoke plume at a distance

of 2.9 km from the lidar ( $SNR \approx 4.5$ ), which was detected through dense clouds located within the range 1–2 km.

## Conclusions

The experiments described demonstrate that the direct-detection single-wavelength lidar technique is a promising method for early forest fire detection. The detection delay within the instrument's detection range is essentially defined by the laser-beam scanning algorithm. Forest-fire detection within a range of 2.5 km can be successfully carried out with a uniform azimuth sweep of  $\Delta\varphi \cong 2^\circ$ , and this scanning rate is achievable with available lidar equipment in about 3 min for a full-circle sweep.

The issue of primary practical importance is how the distance to the fire (or, rather, to the smoke plume),  $R$ , affects the feasibility of forest fire detection. For remote-detection applications, the feasibility is usually estimated on the basis of the signal-to-noise ratio (how pronounced is the desired signal against the noise background). It is supposed that for reliable detection one must achieve  $SNR \geq 5$ . As it is seen from equation (3), describing the  $SNR$  variation with distance, the decay of the retroreflected power  $P_r(R)$ , described by equation (1), is the main potential limitation to lidar-assisted forest-fire surveillance. The signal decay may be reduced, in particular, by increasing the laser pulse energy and/or the photodetector sensitivity. The influence of other factors, such as the concentration of smoke particles, is as well very important. An experimental and theoretical treatment of the basic phenomena affecting the dependence of  $SNR$  on the distance to the smoke plume was carried out in a different paper (Utkin *et al.* 2002). Satisfactory agreement between the experimental  $SNR$  values for smoke plumes and values predicted on the basis of equations (1)–(3) makes it possible to estimate the maximum range of reliable detection ( $SNR \geq 5$  for  $n = 128$ ) for available lidar equipment in good-weather conditions. In Fig. 8 the estimated range curves corresponding to the energy of the laser pulse,  $E_p$ , equal to 5 and 30 mJ, are plotted for the height of the smoke-plume observation equal to 50 and 300 m as a function of the burning rate. The wind velocity was assumed to be zero, and in this condition the backscattering and extinction coefficients of the smoke plume, appearing in equation (1), were calculated for the given burning-rate value with the help of a gas dynamic model described in Vilar and Lavrov (1999).

The model refers to a smoke plume produced by a compact fire source (simulating a starting forest fire) and developing in conditions of flat terrain and still atmosphere. In this case (Fig. 1) while rising, the smoke plume expands and mixes with ambient air. Consequently, the smoke particle concentration and the range for reliable detection decrease when the height to the ground of the laser beam–smoke plume intersection point increases. As is seen from the figure, the estimated values of the range of reliable detection are 10–23 km, similar to or better than the range of best ground-based passive

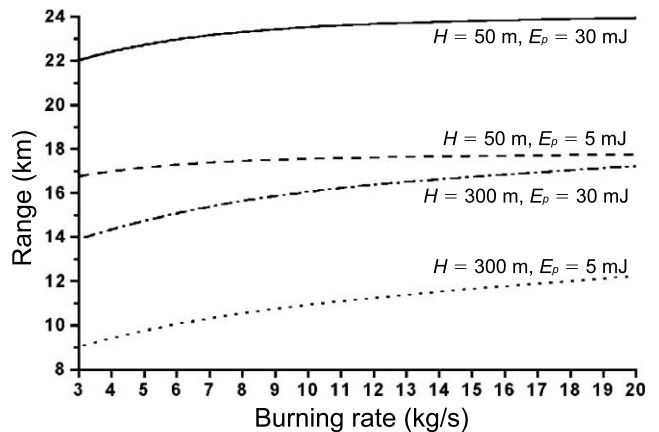


**Fig. 8.** Estimates of the maximum range of reliable detection ( $SNR \geq 5$  for  $n = 128$ ) for the available lidar equipment in the good-weather conditions plotted for two heights of the smoke-plume observation,  $H = 50$  and 300 m, and two energies of the laser pulse,  $E_p = 5$  and 30 mJ.

systems of fire detection (Thomas and Nixon 1993; Ollero *et al.* 1998; Ugarte *et al.* 2000). However, the lidar method presents several clear advantages because it does not require direct visibility of the fire or hot regions of the accompanying gas flow, provides more reliable monitoring due to its better false-alarm rejection capability, and provides accurate identification of the fire location.

It is worthwhile to note that, in further development of the lidar system towards an industrial prototype, the probing laser pulse must be made eye-safe and the algorithm allowing for automatic recognition of the smoke signature in the lidar return curve needs to be developed.

The lidar apparatus described in this paper is not eye-safe. The safe distance for direct eye exposure meeting the ANSI and IEC standards is about 4.5 km. It is clear that simply decreasing the laser-beam energy to the eye-safe threshold would have led to inadmissible lowering of the fire detection range. As it is widely discussed in the literature, there are three means for efficiently meeting eye-safety requirements:

- The simplest way is to use a laser that generates low-energy pulses of eye-safe radiation with very high repetition rate. Collecting and summing a large number of lidar returns per unit time will diminish the noise and compensate the  $SNR$  degradation due to the low backscattered energy. However, only well-uncorrelated noise can be effectively suppressed by data accumulation, which is not the case for some types of atmospheric and detection noise.
- The second way implies distributing the probing-pulse energy over a large beam cross-section through expanding the laser beam. In a monoaxial lidar architecture, the same telescope may be used for both laser-beam expansion and collection of the backscattered energy. Significant beam expansion may even increase the detection range, owing to

- lower beam divergence, but it may result in a more complex and costly equipment.
- The most efficient way of achieving eye-safe operation is using a suitable wavelength, either in the ultraviolet ( $\lambda < 400$  nm) or in the infrared ( $\lambda > 1400$  nm) spectral ranges. The authors considered the latter opportunity in previous publications (Vilar *et al.* 2001; Lavrov *et al.* 2003) and concluded that using an Er:glass laser at a wavelength of 1540 nm and an avalanche photodiode for radiation measurement will allow the design of an eye-safe lidar using the same architecture as described in the present work. For the same laser pulse energy, the 1540 nm Er:glass lidar has better detection range than a 1064 nm or 512 nm Nd:YAG lidar (Lavrov *et al.* 2003).

Development of automatic systems for fire surveillance and lidar signal processing is connected with solution of ill-posed problems that in the last decade were intensively treated with artificial intelligence and neural-network algorithms (Bhattacharya *et al.* 1997; Arrue *et al.* 2000). Remarkably, in the case of lidar applications, the area-surveillance task can be reduced to a set of 1-dimensional problems, each of which addresses the data attributed to a line of propagation of the probing pulse. The work described in this paper provides an experimental base for neural-network technologies. Pronounced smoke signatures obtained for good weather conditions indicate the possibility of constructing the training set for supervised neural-network learning.

## Acknowledgements

This research was partially supported by INTAS grant N. 99-1634. A.B. Utkin gratefully acknowledge financial support from Instituto de Ciéncia e Engenharia de Materiais e Superfícies. A. Lavrov thanks the NATO Scientific Affairs Department for a fellowship grant. A. Fernandes gratefully acknowledges Ph.D. grant SFRH/BD/2943/2000 from Fundação para a Ciéncia e a Tecnologia. The authors are grateful to Professor Xavier Viegas, University of Coimbra, for the invitation to participate in the Gestosa 2001 project and for his help in organising the experiments. The authors acknowledge valuable comments and suggestions of the Referees.

## References

- Andreucci F, Arbolino MV (1993a) A study on forest fire automatic detection systems. 1. Smoke plume model. *Nuovo Cimento* **16C**, 35–50.
- Andreucci F, Arbolino MV (1993b) A study on forest fire automatic detection systems. 2. Smoke plume detection performance. *Nuovo Cimento* **16C**, 51–65.
- Arrue BC, Ollero A, Martinez de Dios JR (2000) An intelligent system for false alarm reduction in infrared forest-fire detection. *IEEE Intelligent Systems* **May/June 2000**, 64–72.
- Banta RM, Oliver LD, Holloway ET, Kropeli RA, Bartram BM, Cupp RE (1992) Smoke-column observation from two forest fires using Doppler lidar and Doppler radar. *Journal of Applied Meteorology* **31**, 1328–1349.
- Benech B, Dinh PV, Ezcurra A, Lesne JL (1988) Investigation of a 1000-MW smoke plume by means of a 1.064  $\mu\text{m}$  lidar. II. Determination of diffusion characteristics of the plume particles. *Atmospheric Environment* **22**, 1071–1084.
- Bennet M, Sutton S, Gardiner DRC (1992) An analysis of lidar measurements of buoyant plume rise and dispersion at five power stations. *Atmospheric Environment* **26A**, 3249–3263.
- Bhattacharya D, Pillai SR, Antoniou A (1997) Waveform classification and information extraction from lidar data by neural networks. *IEEE Transactions on Geoscience and Remote Sensing* **35**, 699–707.
- Bissonnette LR (1986) Sensitivity analysis of lidar inversion algorithms. *Applied Optics* **25**, 2122–2125.
- Bösenberg J, Brassington D, Simon PC (1997) ‘Instrument development for atmospheric research and monitoring.’ (Springer: Berlin) 394 pp.
- Davidson GA, Slawson PR (1982) Effective source flux parameters for use in analytical plume rise model. *Atmospheric Environment* **16**, 223–229.
- Eberhard WL (1983) Eye-safe tracking of oil fog plumes by UV lidar. *Applied Optics* **22**, 2282–2285.
- Fromm M, Alfred J, Hoppel K, Hornstein J, Bevilacqua R, Shettle E, Servranckx R, Li ZQ, Stocks B (2000) Observations of boreal forest fire smoke in the stratosphere by POAM III, SAGE II and lidar in 1998. *Geophysical Research Letters* **27**, 1407–1410.
- Hamilton PM (1969) The application of a pulsed-light rangerfinder (lidar) to the study of chimney plumes. *Philosophical Transactions of the Royal Society of London A* **265**, 153–172.
- Heikes KE, Ransohoff LM, Small RD (1990) Numerical simulation of small area fires. *Atmospheric Environment* **24A**, 297–307.
- Hinkley ED (1976) ‘Laser monitoring of the atmosphere.’ (Springer: Berlin) 381 pp.
- Jelalian AV (1992) ‘Laser radar systems.’ (Artech House: Boston) 292 pp.
- Klett JD (1981) Stable analytical inversion solution for processing lidar returns. *Applied Optics* **20**, 211–220.
- Lavrov A, Utkin AB, Vilar R, Fernandes A (2003) Application of lidar in ultraviolet, visible and infrared ranges for early forest fire detection. *Applied Physics B* **76**, 87–95.
- Longo KM, Thompson AM, Yamasoe MA (1999) Correlation between smoke and tropospheric ozone concentration in Cuiaba during Smoke, Clouds, and Radiation-Brazil (SCAR-B). *Journal of Geophysical Research* **104**, 12 113–12 119.
- Measures MR (1984) ‘Laser remote sensing.’ (Wiley: New York) 510 pp.
- Muller D, Wagner F, Althausen D, Wandinger U, Ansmann A (2000). Physical properties of the Indian aerosol plume derived from six-wavelength lidar observations on 25 March 1999 of the Indian Ocean Experiment. *Geophysical Research Letters* **27**, 1403–1406.
- Netterville DDJ (1990) Plume rise, entrainment and dispersion in turbulent winds. *Atmospheric Environment* **24A**, 1061–1081.
- Ollero A, Martinez de Dios JR, Arrué BC (1998) Integrated systems for early forest-fire detection. Proceedings of III International Conference on Forest Fire Research and 14th Conference on Fire and Forest Meteorology. University of Coimbra, Luso, **II**, 1977–1988.
- Pershin S, Hao WM, Susott RA, Babbitt RE, Riebau A (1999) Estimation of emission from Idaho biomass fires using compact eye-safe diode lidar. *Proceedings of SPIE* **3757**, 60–66.
- Pratt WK (1969) ‘Laser communication systems.’ (Wiley: New York) 271 pp.
- Roberts SD, Dean TJ, Evans DL (2003) Family influences on leaf area estimates derived from crown and tree dimensions in *Pinus taeda*. *Forest Ecology and Management* **172**, 261–270.
- Saito Y, Saito R, Kawahara TD, Nomura A, Takeda S (2000) Development and performance characteristics of laser-induced fluorescence imaging lidar for forestry applications. *Forest Ecology and Management* **128**, 129–137.

- Targ R, Steakley BC, Hawley JG, Ames LL, Forney P, Swanson D, Stone R, Otto RG, Zarifis V, Brockman P, Calloway RS, Klein SH, Robinson A (1996) Coherent lidar airborne wind sensor. *Applied Optics* **35**, 7117–7127.
- Thomas PJ, Nixon O (1993) Near-infrared fire detection concept. *Applied Optics* **32**, 5348–5355.
- Ugarte MF, Castro AJ, Briz S, Aranda JM, López F (2000) Optimized geometry in infrared arrays for remote sensing of forest fires. *Infrared Physics & Technology* **41**, 35–39.
- Uthe EE (1981) Lidar evaluation of smoke and dust clouds. *Applied Optics* **20**, 1503–1510.
- Uthe EE, Morley BM, Nielsen NB (1982) Airborne lidar measurements of smoke plume distribution, vertical transmission, and particle size. *Applied Optics* **21**, 460–463.
- Utkin AB, Lavrov AV, Costa L, Simões F, Vilar R (2002) Detection of small forest fires by lidar. *Applied Physics B* **74**, 77–83.
- Viegas X (2000) Gestosa 2000. Experimental fires in shrub vegetation in Central Portugal. *International Forest Fire News* **23**, 102–105. [Information on Gestosa 2001 is also available at <http://www.geo.unizh.ch/gis/research/edmg/fire/gestosa01/index.html>.]
- Vilar R, Lavrov A (1999) Application of lidar at 1.54 micron for forest fire detection. *Proceedings of SPIE* **3868**, 473–477.
- Vilar R, Lavrov A (2000) Estimation of required parameters for detection of small smoke plumes by lidar at 1.54 μm. *Applied Physics B* **71**, 225–228.
- Vilar RM, Lavrov AV, Utkin AB, Fernandes A (2001) Comparison of eye-safe UV and IR lidar for small forest fire detection. Technical Program and Final Summary Digest, 8th International Symposium on Remote Sensing, Conference 4542 *Remote Sensing for Agriculture, Ecosystems, and Hydrology III*, Toulouse, pp. 17, 123.
- Wei H, Koga R, Iokibe K, Wada O, Toyota Y (2001) Stable inversion method for a polarized-lidar: analysis and simulation. *Journal of the Optical Society of America A* **18**, 392–398.
- Weinman JA (1988) Derivation of atmospheric extinction profiles and wind speed over the ocean from a satellite-borne lidar. *Applied Optics* **27**, 3994–4001.
- Youmans DG, Garner R, Peterson KR (1994) Dust cloud density estimations using a single wavelength lidar. *Proceedings of SPIE* **2271**, 13–28.
- Zuev VE, Naats IE (1983) ‘Inverse problems of lidar sensing of the atmosphere.’ (Springer: Berlin) 260 pp.